

Towards an accurate brain tractography using diffusion weighted imaging

Eleftherios Garyfallidis
Supervisor: Ian Nimmo-Smith

26th June 2009

Medical Research Council
Cognition and Brain Sciences Unit

Contents

1	Introduction	2
1.1	Terminology	2
2	Diffusion Weighted Imaging signal	3
2.1	What is diffusion?	3
2.2	Diffusion Maths	3
2.3	Acquisition sequences in use	5
2.4	What is a b-value?	6
2.5	What is DWI?	7
3	Q-space methods	7
3.1	What is q-space?	7
3.2	Acquisition methods and defining terms	9
4	Deterministic vs Probabilistic Tracking	10
5	Software	12
6	FA Results	13
6.1	Trichotillomania	13
7	Tractography Results	15
7.1	HARDI Experiments in CBU	15
8	Future Plan	15
9	Conclusion	18
10	Acknowledgements	18

11 Appendix	19
11.1 Problems for fiber tracking	19
11.2 Motion and Eddy Correction	19
11.3 Comparing across subjects	19
11.4 TBSS	20
11.5 Visualising local estimates of diffusion direction	21
11.5.1 Tensor models	21
11.5.2 Spherical Harmonic Models	22
11.5.3 Model free	22

1 Introduction

Diffusion MRI (dMRI) is the only non-invasive method that provides information about the neural tracts found in white matter and the cortex. dMRI acquires one or more T2-weighted reference images, and a collection of diffusion-weighted images that attenuate the T2 signal according to the amount of diffusion along prescribed gradient directions [30]. The information is not complete and the tracts cannot be reconstructed in full detail [22]. However, some spatial structures and patterns can be visualised. These are usually represented as trajectories[57] or connectivity maps [10]. The unique new area that aims to reconstruct the neural tracts from diffusion data is called diffusion tractography. Other types of tractography are based in staining using for example luxol-fast blue [39] but these can only be used with in vitro brains and they lack ease of repeatability.

The field of diffusion tractography is less than ten years old. It started with Mori's first tractography algorithm FACT[42] in 99 and it is still under massive research and development. We believe that the resolution and accuracy of tractography today is weakened by the following problems:

1. Poor acquisition schemes not specifically designed for tractography.
2. Over-simplistic local fiber direction modelling.
3. Lack of gold standard phantoms and validation techniques for dMRI.
4. Lack of robust and efficient tractography algorithms.

The goal of this thesis is to investigate possible solutions or improvements of existing solutions for all four problems. However, we focus more on problems 2 and 4. We want to be able to increase the resolution of tractography taking into account global properties of the brain. We believe that by using whole brain discrete optimisation and Bayesian inference we will be able to remove many artifacts and ghosts, see section 8. In order to decide which is the best way to go forward and plan our research strategy we had to study and test many different algorithms and approaches (see sections 4 and 6) and gather data sets obtained at the MRC-CBU (see Fig. 1,2) and elsewhere. Furthermore, we developed a new software library in Python which is able to visualise and interact with 3D/4D data sets, open medical files, calculate tensors, draw trajectories, and many other features, see section 5. We proposed and tested a new acquisition protocol that will hopefully replace the current default dMRI protocol in MRC-CBU, for more details see 7.

1.1 Terminology

Diffusion imaging has many terms, and one source of confusion has been lack of clarity in the meaning of these terms. To start, we will use the term “diffusion weighted imaging” (DWI) to refer to any MRI image acquisition that is weighted to be sensitive to diffusion.

One major source of confusion is that terms are often used to refer both the type of *acquisition* used to acquire the data, and to the subsequent *analysis* of the data. The most egregious example is the term “diffusion tensor imaging” (DTI). Used in a technical sense, the term refers to a very simple analysis model for the per-voxel diffusion direction profiles - a single diffusion tensor (SDT). However, it is also used to refer to all diffusion weighted imaging, or to a particular type of acquisition with a small number of diffusion gradient directions (of

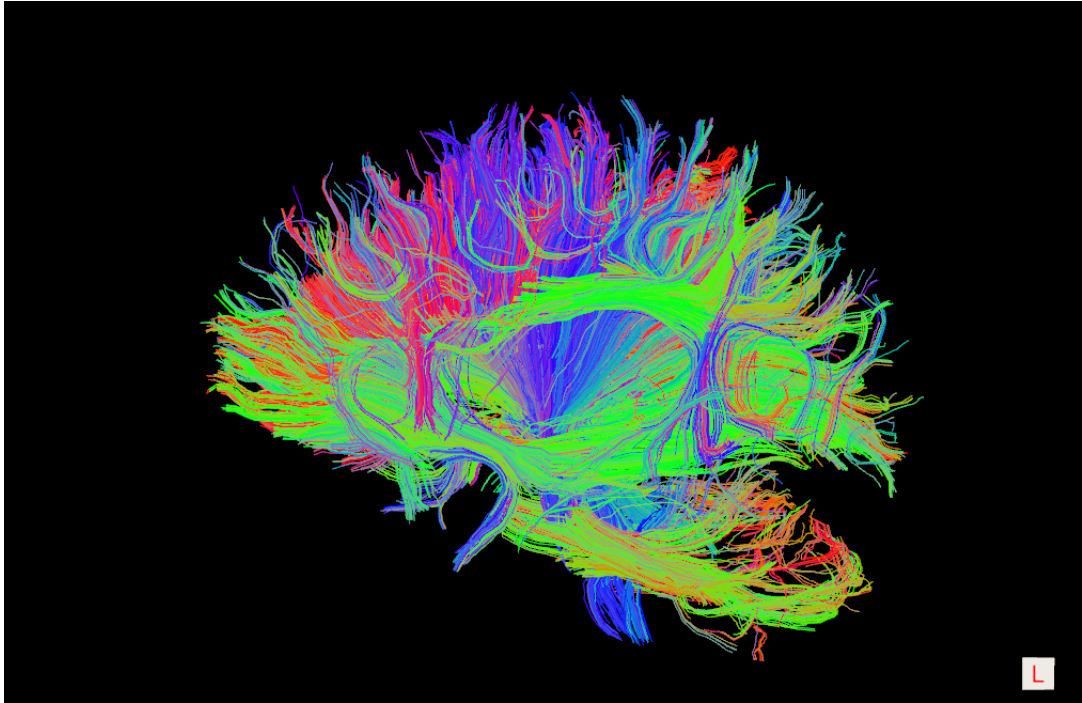


Figure 1: These results were obtained at MRC-CBU and analyzed with DTK & TrackVis with the option using the deterministic algorithm FACT. All tracts smaller than 26 mm were removed. See sections 4 and 7 for discussion and Fig.2 for comparison.

which more below). We will avoid the term DTI in this paper, and humbly suggest that it will reduce confusion if others do the same.

Tractography is the process of spatially integrating local estimates of fiber directions throughout the brain. Tractography gives only an estimation of the real tracts. Consequently, when using the term tracts it will probably mean computational tracts or tracks, i.e. trajectories, except if it is stated as actual tract or existing tract. The terms tract and fiber are considered here equivalent.

2 Diffusion Weighted Imaging signal

2.1 What is diffusion?

Diffusion here implies molecular diffusion. Molecular diffusion is the phenomenon observed when molecules move from regions of higher concentration to regions of lower concentration using random movement. Usually, this happens inside fluid. The result of diffusion is a gradual mixing of material and entropy maximisation where the molecules tend to take the shape of the container containing the fluid. Anisotropy is one of the terms that are very common in diffusion terminology. Anisotropy means that the average displacement of the particles will move towards a specific direction. On the other hand, isotropy means that the particles are equally likely to move in any direction. In dMRI the protons will move more towards the directions of the axons and less vertical to the direction. For a biological interpretation of the signal measured with dMRI see[8] , [59] and [30].

2.2 Diffusion Maths

Fick's two laws are generally used to approximate diffusion and Einstein was one of the many scientists who contributed to the understanding of these laws [25]. From Fick's first law flux J is equal to the inverse of the gradient of concentration C

$$J = -D \nabla C \quad (1)$$

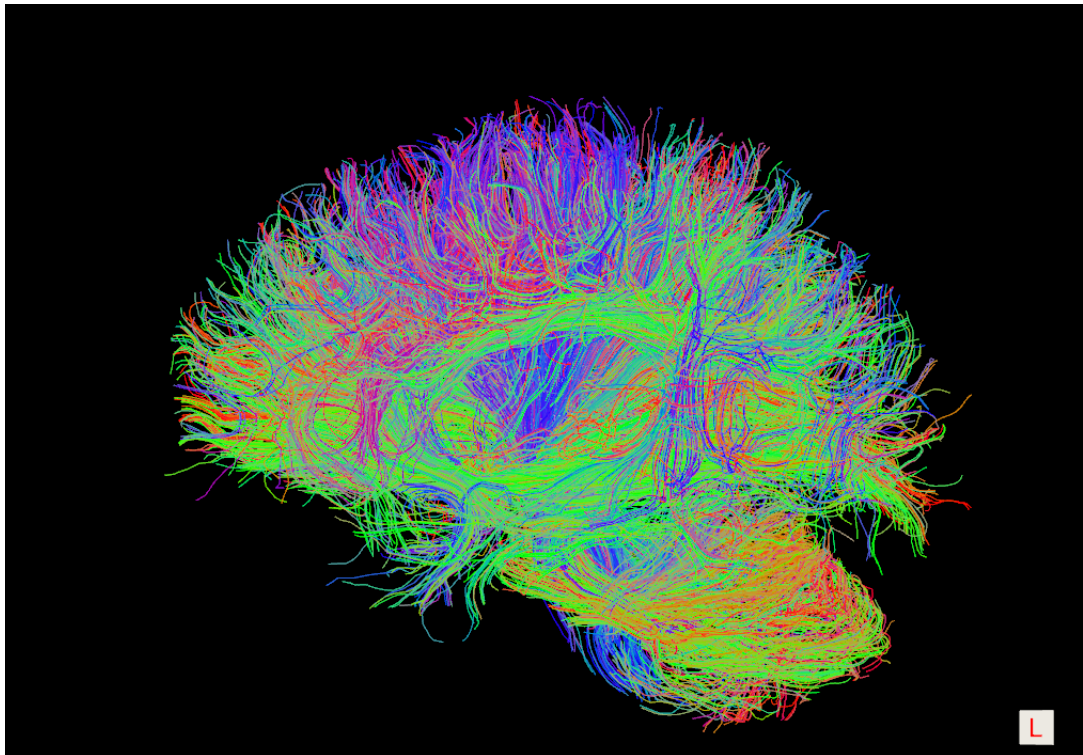


Figure 2: Similar with Fig. 1 but here the deterministic algorithm R-K was used with the same 26 mm threshold. By comparing these two figures it is obvious that R-K generated thousands more tracts than FACT. So, which one is the best? The need for validation of existing tractography and the removal of ghost tracks is crucial for obtaining meaningful data. However, this is a very difficult problem for which we hope to spend our time investigating possible solutions and inventing new more accurate tractography algorithms.

where D is the diffusion coefficient. Fick's second law derives from the conservation of mass

$$\partial C / \partial t = D \nabla^2 C \quad (2)$$

and it just shows that when we have changes in concentration matter moves in or out of the container. This last differential equation is also known as the diffusion equation. When a molecule is at position x_0 , we cannot say where it will be after time t , we can only model a distribution of locations. This motion is described by a propagator $P(x; x_0, t)$ which defines the probability of being in x after a time t , starting at x_0 .

The orientation distribution function (ODF) expresses the probability of a spin displacing into a differential solid angle about a fibre direction u . This is used in order to visualise the diffusion propagator and in simple words it just projects the diffusion function on to the sphere by integrating over the radial coordinate of the diffusion function. The ODF representation symbolised below with f sacrifices all the radial information but retains the relevant directional information:

$$f(\mathbf{u}) = \int_0^\infty P(\rho \mathbf{u}) d\rho \quad (3)$$

where \mathbf{u} is a unit normal vector and ρ is the radial coordinate in the diffusion space. Stejskal and Tanner [54] showed that the spin echo magnitude $S(\mathbf{q}, t)$ from a PGSE experiment is directly related with the diffusion propagator by the following Fourier relation

$$S(\mathbf{q}, t) = S_0 \int P(\mathbf{R}, t) e^{i\mathbf{q}^T \mathbf{R}} d\mathbf{R} \quad (4)$$

where S_0 is the signal in the absense of the applied diffusion gradient, \mathbf{R} is the relative spin displacement $\mathbf{x} - \mathbf{x}_0$ at diffusion time t , \mathbf{q} is the spin displacement wave vector. With the inverse Fourier transform we can reconstruct the diffusion propagator P by measuring the signal in different directions. Q-space imaging (QSI) and Diffusion Spectrum Imaging (DSI) are the best known methods which try to reconstruct the full diffusion propagator in that way.

Assuming that the diffusion propagator is given by a Gaussian distribution we can write

$$P(\mathbf{R}, t) = \frac{1}{\sqrt{4\pi t^3 |\mathbf{D}|}} \exp\left(-\frac{\mathbf{R}^T \mathbf{D}^{-1} \mathbf{R}}{4t}\right) \quad (5)$$

where \mathbf{D} is known as the diffusion tensor. This tensor is a 3D symmetric matrix that can be completely described by a centred ellipsoid with axes $\lambda_1, \lambda_2, \lambda_3$. Fractional Anisotropy (FA) is a very common metric in diffusion imaging which is calculated from these values.

$$FA = \frac{1}{\sqrt{2}} \frac{\sqrt{(\lambda_1 - \lambda_2)^2 + (\lambda_2 - \lambda_3)^2 + (\lambda_3 - \lambda_1)^2}}{\sqrt{\lambda_1^2 + \lambda_2^2 + \lambda_3^2}} \quad (6)$$

If FA is equal to 1 that means very anisotropic (infinitely prolonged ellipsoid) and if FA is equal to 0 that means totally isotropic (sphere). FA is used in clinical studies to diagnose diseases like stroke and cancer and asses the progress of therapy [38].

Whenever we are using FA volumes we assume that the propagator of the spins in every voxel will be a 3D Gaussian distribution. This assumption is used in most of diffusion related publications. Unfortunately, in reality things are much more complicated; inside our brain the axons are semi-permeable (restriction), the water molecules interact with many different elements in the complex intra fibre fluid, the fibres might cross, kiss, divert or bent inside a voxel. Therefore, assuming a Gaussian distribution is a non-trivial approximation. For alternatives see 3.

2.3 Acquisition sequences in use

The best known method for generating diffusion-weighted images is called Pulsed Gradient Spin Echo method (PGSE), also known as the Stejskal and Tanner method [54]. This has 90-180 degrees spin echo pair of RF pulses with one gradient before the second pulse and one equal gradient after the second pulse (see [40], p329),

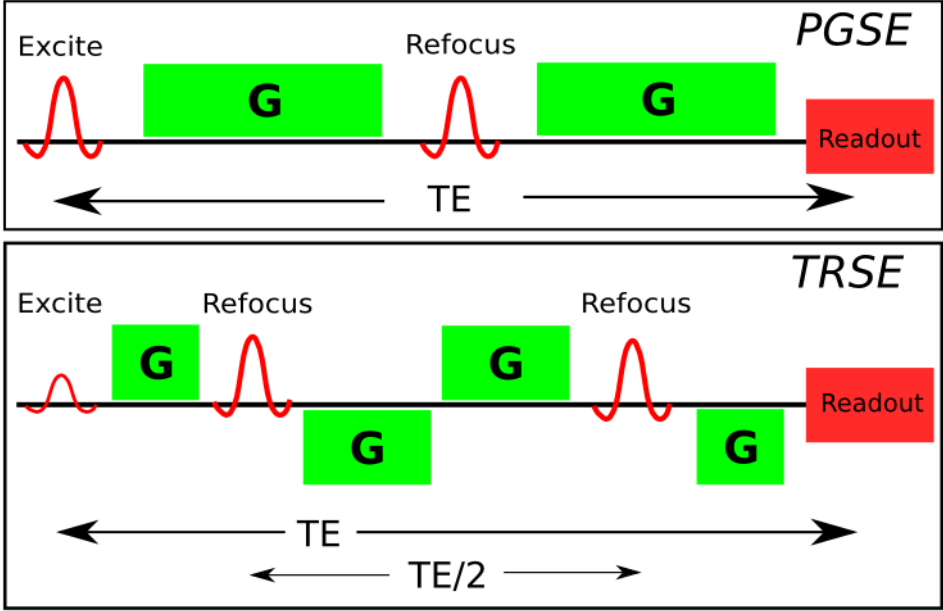


Figure 3: PGSE and TRSE

see Fig. 3. The refocusing is perfect only when the spins do not move between the two pulses. The diffusion weighted contrast acts like inverse T_2 weighting i.e. tissues with mobile water molecules give lower signal than more solid tissues with smaller mobility. Eddy currents caused by the onset and offset of the gradients are a problem with PGSE and most systems (including Siemens) use twice-refocused spin echo sequences [50] to reduce these artifacts. Every time the magnetic field gradients switch they generate currents that generate other smaller magnetic fields which disturb the spins. The TRSE sequence is an improvement on the PGSE. The improvement is made using another refocusing pulse surrounded by the inverse mirror of the previous diffusion gradients (see Fig. 3). By adjusting the timing of the diffusion gradients, eddy currents can be nulled or greatly reduced. This sequence improves the image quality without loss of scanning efficiency i.e. TR duration and it is the standard in most modern MRI scanners.

2.4 What is a b-value?

The b-value b is a function of the strength, duration and temporal spacing and timing parameters of the specific paradigm. This function is derived from the Bloch-Torrey equations[15]. In the case of the classical Stejskal-Tanner pulsed gradient spin-echo (PGSE) sequence, at the time of readout

$$b = \gamma^2 G^2 \delta^2 \left(\Delta - \frac{\delta}{3} \right),$$

where γ is the gyromagnetic ratio, δ denotes the pulse width, G is the gradient amplitude and Δ the centre to centre spacing. γ is a constant, but we can change the other three parameters and in that way control change the b-value.

Under the Brownian motion assumption the signal strength is described by the equation $S(b) = S(0)\exp(-bD)$ where D is the diffusion coefficient that we wish to measure and b the crucial experimental parameter diffusion weighting parameter or b-value which summarises the diffusion sensitising gradient history. Although the PGSE is useful for expository clarity, in reality more complicated but related sequences such as the twice-refocused spin-echo (TRSE) [29, 50] sequence and subsequent refinements such as TRASE [3] are employed as a means of removing the distortion effects from eddy currents resulting from the initial and final ramps of the gradient pulses. The important point is that we can control the size of the b-values by changing the strength and timings of the gradient pulses and that depending on the b-value, we can expect different amount of signal loss. A further important simplifying assumption that us made is that the function $S(b)$ is described by a single exponential term (mono-exponential). In fact there is evidence that this assumption may break down at higher

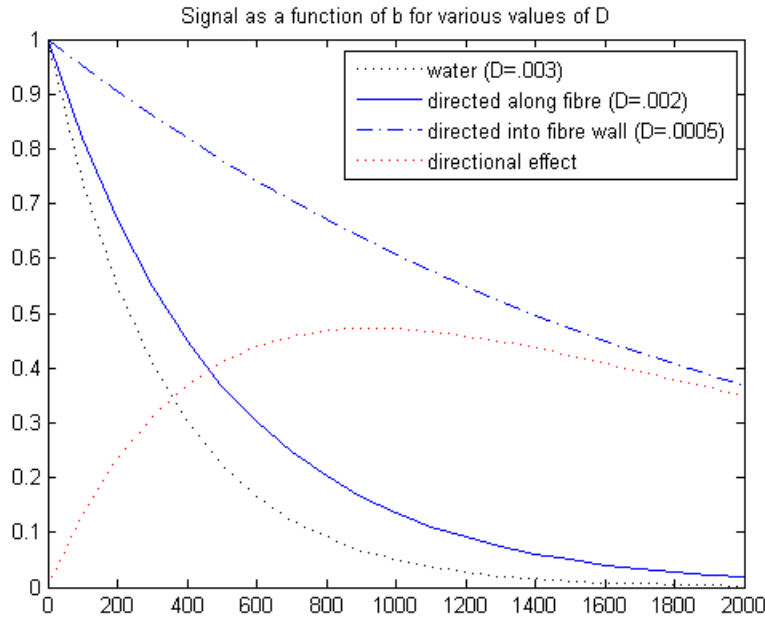


Figure 4: Signal as a function of b for various values of D

b -values. The units of D are mm^2/sec (for water at $37^\circ D \approx 3 \cdot 10^{-3} m^2/sec$), and of b are sec/mm^2 , typically in the range $0\text{--}5,000 sec/mm^2$ though some DW-MRI acquisition paradigms can call for very much larger values e.g. $12,000 sec/mm^2$.

2.5 What is DWI?

Diffusion Weighted Imaging (DWI) is MRI imaging designed to be sensitive to diffusion. With this imaging technique we can delineate the axonal organisation of the brain. A diffusion weighted image is a volume of voxels gathered by applying only one gradient direction to our sequence. Therefore, the signal in every voxel should be low if there is motion of water molecules towards the specified the gradient direction or it should be high if there is less movement in the same direction. Therefore if inside a voxel there is an underlying fibre that is parallel to this direction we should expect a lower value otherwise if the fibre is not parallel or near parallel or if there is no underlying fibre we should expect a higher value.

The directional dependence of the DWI signal is the cornerstone of diffusion based tractography. Signal from a specific voxel will be higher in directions where diffusivity is high, e.g. along the direction of a putative bundle of fibres, and lower into the walls of the constituent fibres. Figure 5 and 2.5 show how signal for an anisotropic Gaussian diffusion would change with gradient direction.

3 Q-space methods

3.1 What is q-space?

Q-space is the space of one or more 3D vectors \mathbf{q} as shown in equation 4. This vector is obtained by the formula $\mathbf{q} = (2\pi)^{-1}\gamma\delta\mathbf{g}$. Every single vector \mathbf{q} has the same orientation of the direction of diffusion gradient \mathbf{g} and length proportional to the strength of the gradient g . Every single point in q-space corresponds to a 3D volume of the brain for a specific gradient direction. Therefore if for example we have programmed the scanner to apply 60 gradient directions then our data should have 60 diffusion volumes with each volume obtained for a specific gradient including 1 or more non-diffusion weighted volumes with no applied gradient. A Diffusion Weighted Image (DWI) is the volume acquired from only one direction gradient. Hence, in the previous example we would gather 60 DWI volumes. An alternative way to see \mathbf{q} is in mathematical terms as the combination

Signal as a function of direction for a gaussian diffusion function
with a horizontal principal direction and two values of b

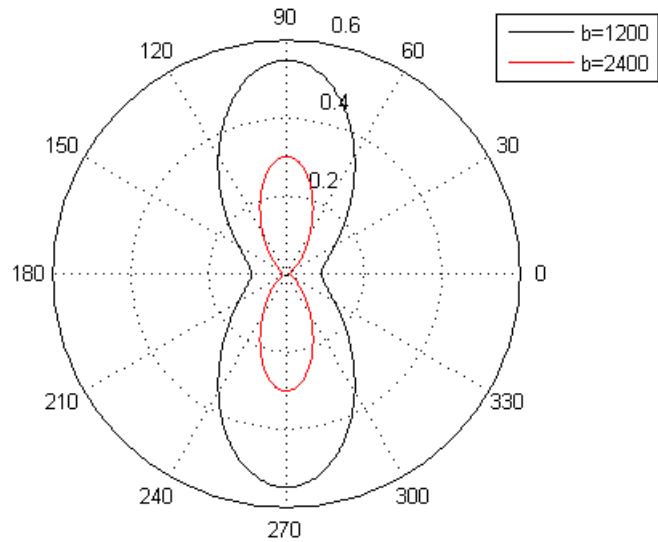


Figure 5: Directional dependence of signal for two b-values

-Log(signal as a function of direction for a gaussian diffusion function
with a horizontal principal direction and two values of b

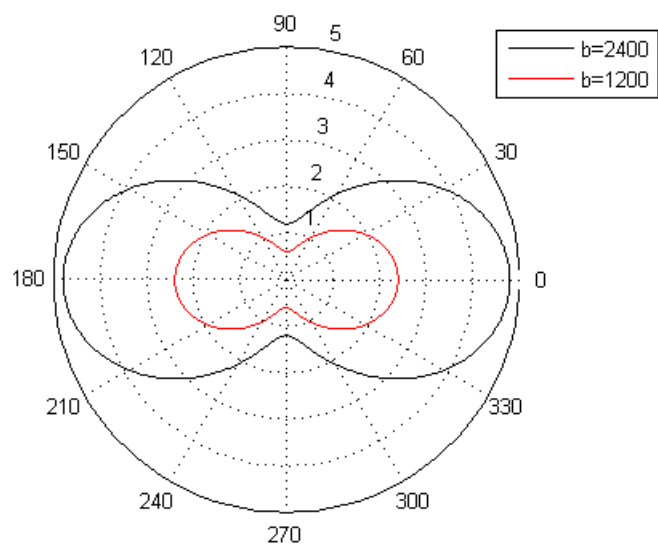


Figure 6: Minus log(signal) of the above

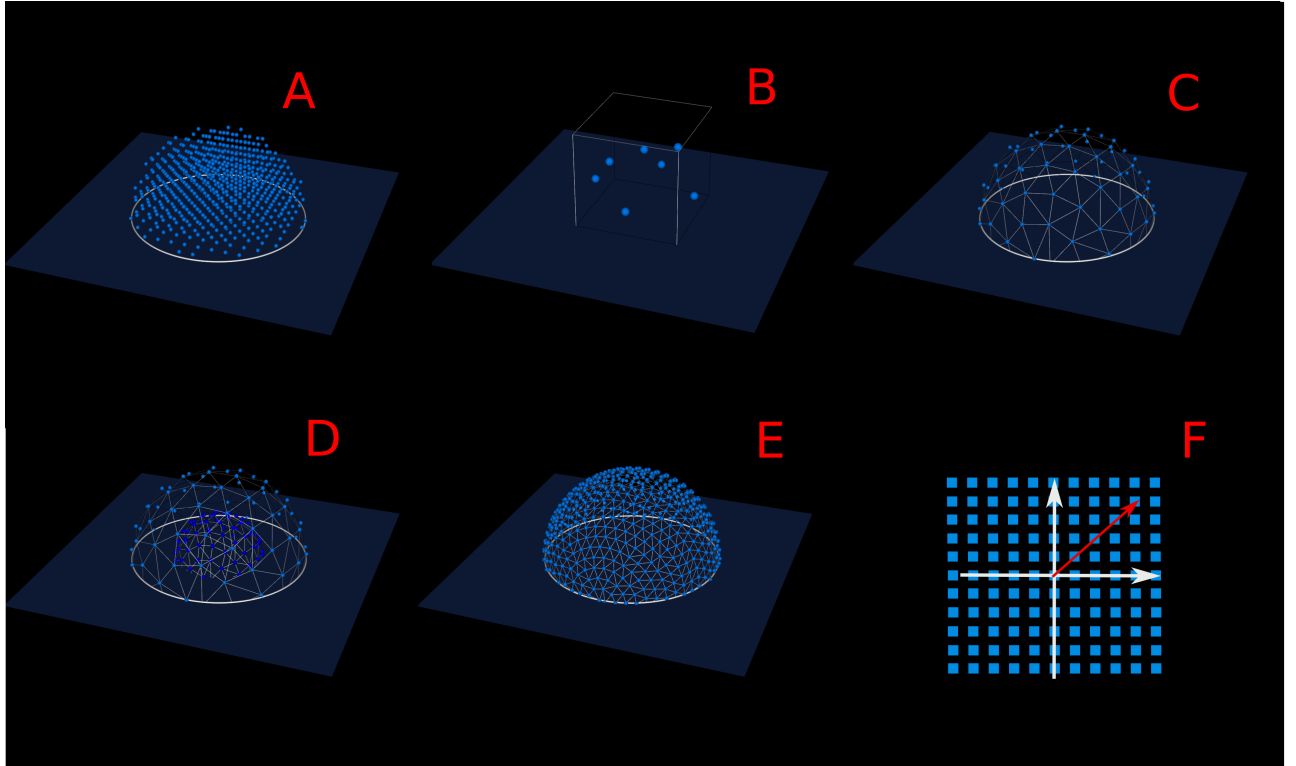


Figure 7: A: DSI 604 directions, B: DTI using only 7 directions, C: HARDI 65 directions, D: HARDI with 2 shells of 65 directions in each shell, E: QBI 515 directions, F: QSI simplified 2D example showing that the full q-space is needed for the reconstruction of the propagator.

of parameters which produces a Fourier transform relationship between the diffusion signal and the probability displacement distribution.

Another way to represent dMRI is the following. We can combine all the DWIs together creating a new multidimensional image where each voxel corresponds to a density of diffusion signals measured in all possible gradient directions \mathbf{g} . This is the only known way to represent all different acquisition methods with the same structure and we are planning to use it for our tractography algorithm (see section 8 for more).

3.2 Acquisition methods and defining terms

In our introduction, we promised to be as clear as possible about the terms we use. One problem in diffusion imaging is that names for techniques often refer both to a particular type of imaging acquisition, and to the subsequent analysis model (see section 11.5). All dMRI acquisition methods acquire data in q-space, but the methods can be categorised by the trajectories they follow in q-space.

We refer to a method as a *q-space shell* method if it is an acquisition method collecting a series of points in q-space that can be thought of as being on a curved surface, typically a sphere. Examples include techniques referred to as HARDI (High Angular Diffusion Imaging), Q-ball Imaging and HYDI (Hybrid Diffusion Imaging). A q-space shell method might involve a collection of a single shell (Fig. 7C,E), e.g. QBI or multiple shells (Fig. 7D) e.g. EQBI. In clinical settings where we can only use a few directions (less than 60 with minimum 6) the only way is to use the SDT model (Fig. 7B).

A *q-space volume* method is an acquisition method that is more easily thought of as collecting points distributed through a volume in q-space. The characteristic example is DSI (Fig. 7A). and QSI(Fig. 7F).

4 Deterministic vs Probabilistic Tracking

The number of different tractography algorithms for diffusion MRI data that have been introduced the last years is enormous and impossible to discuss all here. However, we will begin decrypting here the simplest or most popular deterministic approaches and then we will concentrate to the probabilistic approaches. A tractographic algorithm belongs to the probabilistic domain if the fibre model that is being used is assuming uncertainty i.e. mistakes in the orientation of the fibre at every voxel. If it does not assume any uncertainty along the path of the track then it is deterministic. All tractography algorithms are based in local estimates of diffusion direction. For more information about different models of local estimates see Appendix 11.5.

One of the simplest and first deterministic methods is called fibre assignment by continuous tracking (FACT) [42]. The FACT algorithm starts through the input of an arbitrary point in the volume and then tracks in both directions e.g. forward and backwards. The interesting part with these tracking methods is how they decide when to stop tracking. FACT is using a single threshold variable $R = \sum_i^s \sum_j^s |\mathbf{e}_i \cdot \mathbf{e}_j|/s(s - 1)$ where s is the number of neighbouring voxels and \mathbf{e} is the eigenvector corresponding to the largest eigenvalue in each point. The simplest case for defining a neighbourhood of a voxel is to use all 26 other adjacent (touching) voxels. Now, let's think of how R will behave in different neighbours. When adjacent fibres are aligned strongly R will increase as the absolute value of the dot product grows bigger as the normalised vectors become more co-linear. On the other side, R will grow shorter in regions without continuity in fibre direction, where $R = 0$ in perfect isotropic conditions. In voxels with R less than a prespecified threshold e.g. 0.8 the tracks will stop being followed and FACT will terminate. An important problem with FACT is that it fails to track axons leaving major pathways where it tracks only one of the branches.

Another popular deterministic approach very much inspired by the field of fluid dynamics was introduced by Basser [6] assuming again a continuous vector field but now the tract is generated by the solution of a system of differential equations subject to an initial condition, the position of the seed point. The solution of the system of ordinary differential equations (ODE) is given by an iterative method called 4thorder Runge-Kutta scheme. Here the authors propose that a fibre can be represented by a 3D curve \mathbf{r} parametrised by the arc length s of the track. The iterative solution of this equation $d\mathbf{r}/ds = \mathbf{e}$ generates the trajectory of the underlying fibre also known as streamline.

Basser's method again is very sensitive in local noise and smoothing. However, it is very straightforward and fast. Wedeen et al.[57] showed that we could get vector \mathbf{e} from the local maximum of the ODF calculated in each voxel. In that way we could visualise crossing distributions and depict crossing fibres. The results in [57] show that, using Fourier reconstruction or Funk-Radon analysis on q-space shells, we can generate much richer axonal architecture than SDT models i.e. many more fibres of complex or simple configuration. This investigation suggests that diffusion MRI with sufficient SNR could make tractography a mathematically well-posed problem. However, we need many hours of scanning to reach the necessary resolution.

Other deterministic approaches can be found here [37], [19]. A latest deterministic algorithm called Tensorlines share the problems of the other deterministic algorithms by failing in relatively sharp turns and Meyer's Loop. In summary, the deterministic algorithms generate paths by making a series of discrete locally optimum decisions. These are fast, simple and easy to interpret. Usually, we depict them using streamlines. A streamline is a curve that is always tangent to the velocity vector of the flow. The disadvantages of deterministic algorithms are that a pathway either exists or not (no uncertainty) and that they do not explore the entire space of likely white matter tracts. In other words, local thresholding makes our tractography vulnerable to small noise aberrations. Probabilistic tractography is meant to deal with this problem and generate tracks even in regions that tracking is unclear. This is possible by assuming that uncertainty exists concerning the orientation of the fibre at each point of the track. We will try to illustrate the difference between the two approaches using a simplified 2D example shown in Fig. 8 (i,ii). Generalising afterwards in 3D is straightforward.

Lets imagine that we have a 2D slice where in each pixel we have calculated a vector showing the primary direction for that specific pixel. This vector \mathbf{e} could have been calculated from the tensor as the primer eigenvector or as a primer direction of a different model e.g. the maximum point of the ODF. Lets now think that we want to find the best path from seed A to seed Z. When using deterministic tractography we are using only the local direction information in every pixel therefore in a direction field as this of Fig. 8(i) we will have to use only one track and this is the diagonal pathway with yellow colour. However there are other possible tracts as well in this diagram e.g rather than taking the diagonal go first up north from A and then right. Probabilistic tractography

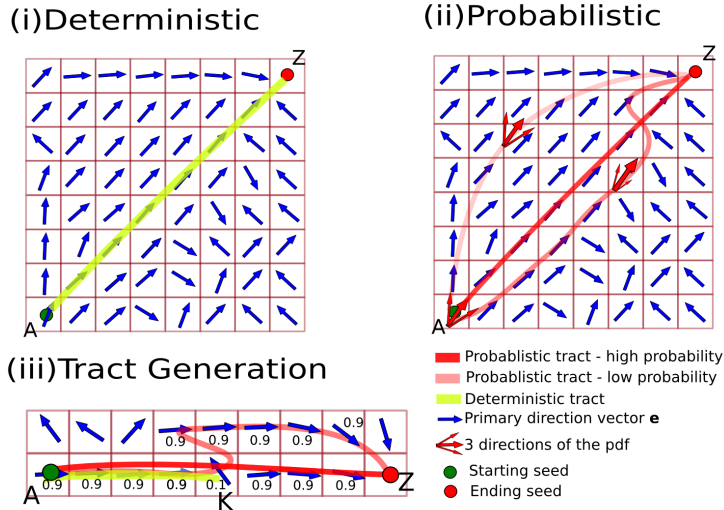


Figure 8: A simplified example showing in (i) & (ii) the same data set but in (i) the yellow line shows the result of deterministic tractography which is given by a single trajectory and in (ii) is given by connectivity matrix depicting with red the probability of different pathways throughout the hole slice. Here only 3 possible pathways are depicted for the ease of understanding. Finally, in (iii) an example is given where it shows that probabilistic tractography weights more closer connections. However it can tract further deep than deterministic tractography. See section 4 for more.

aims to identify all the possible tracts by assigning to each one of them a weight. All the weights of all the tracts together sum to 1. This is possible by generating samples from a probability distribution for every pixel. In this toy example shown in Fig. 8(ii) the orientation of the blue vectors can be represented by a single parameter, angle ω . ω here is a random variable that takes values from a probability distribution function (pdf). Now we have many possible directions to move next but with different probabilities. The weights of all directions again sum to 1. After this explanation we can identify in Fig.8(ii) that the most likely tract is again the diagonal (with deep red) but there are other pathways (with lighter red) that are less likely. In the same diagram we show with 3 combined red arrows some of the many directions that are possible in each point. However, some are more certain than others.

Lets try now to understand how a tract is valued as more probable than others. In 8(iii) we have drawn a very simple image with only two pixel rows and we are assuming that the probability of moving along the primary direction (shown with blue arrow) is 0.9 and there is only a secondary direction given by 0.1 (1-0.9) i.e. we assume for ease of understanding here only 2 directions. We can see that there is a discontinuity in position K. In that point an Euler based deterministic approach would have to stop at K (see yellow line). The probabilistic method will continue tracking and it will generate two tracts that both reach the target. To probability of each tract is calculated by multiplying the probability of a specific direction of each point. Therefore, the shorter and dark red path will have $p_s = 0.9^7 \times 0.1$ and the longer and lighter red path will have $p_l = 0.9^{10}$. It is obvious that $p_s > p_l$ and that the darker red path is more likely to exist according to this method.

This method of multiplying the probabilities at each voxel along the paths has been proposed by many [26],[2], [13], [27],[31],[?], [47] and used in many software packages as well as Parker's PICO[45] in Camino , Berhens' FDT [11, 9, 10] in FSL, and others.

Although the probabilistic methods are able to identify many known tracts, they miss several large tracts such as the visual pathways LGN-MT and callosal MT. The visual pathways are useful frameworks for algorithmic development and testing because they diverge and bend significantly. The current methods have the advantages that they expand the track search space beyond deterministic algorithms and that they can easily expand with complex models supporting crossings (usually not more than 2 crossings). However, they don't compute an accurate probability of brain connections. The statements "Connection probabilities" or "estimation of global connectivity" or "the probability of the existence of a connection through the data field, between any two distant points" found in [11] can be very misleading because someone might believe that they represent the actual connectivity profile of the subject. For example we are certain (with probability 1) that LGN (lateral

	Deterministic	Probabilistic
Voxel Noise Resistance	More	Less
Non-existing Tracts	Yes	Yes
Execution Time	Fast	Slow
Memory Size	Less	More
Biased on Tract Length	No	Yes

Table 1: Deterministic vs Probabilistic Tractography

geniculate nucleus) is connected to V1 and V2 (primary visual cortex) in a healthy brain however the estimated connection probability in FDT is much less than 1. In addition, current probabilistic algorithms fail to identify pathways even when they are known to exist or in a few cases they generate pathways even when they do not exist [12, 33, 52]. For example no connections between left MT+ and the posterior portion of Corpus Callosum were found in PiCo [45] or FDT although it is well established that they do exist.

In 2008 Sherbondy [53] in order to try to deal with the problems explained in the previous paragraph implemented in ConTrack an algorithm that separates the pathway sampling and scoring steps. In that way the scoring does not depend any more on whether we are tracking from seed A to seed B or from B to A therefore, it assumes symmetry when the other probabilistic methods do not. At the same time Sherbondy’s method assumes independence between different tracts i.e. path $A \rightarrow B$ is independent from $A \rightarrow C$ or $K \rightarrow L$. This is not happening in most other methods where the pathways depend on other pathways starting from the same seed. So, ConTrack is designed to estimate connections that are known to exist. The disadvantage of Sherbondy’s method is that it needs a lot of user interaction to add the known tracks and the user needs to be a specialist in white matter anatomy otherwise the results might be biased. The same problem exists with the waypoint masks used in the latest versions of FDT. Finally, a tiny summary of the plus and minus of different tractography is given in Table 1.

5 Software

We write our software in Python with embedded C/C++ modules for speed if necessary. We choose Python because it is open source, multiplatform, free, it has a very simple object oriented syntax and many interfaces with GUIs, scientific computing libraries and other languages. We also hope that some of our code will be used in a future version of Nipy. We coined the name Tractarian (TRN) for this python project but there are many functions and files that are useful not only for tractography but generally for machine learning, scientific visualisation and medical imaging. TRN consists of the following modules diffusion.py, art.py, lights.py, form.py, eyes.py and external.py. See Table 2 for a summary of their features.

In more detail lights module using underneath the Visualisation Toolkit (VTK) library provides simple commands to generate cones, tori, cubes, points, point clouds(dots), spheres, lines, poly-lines, trajectories, labels, arrows, planes, axes, splines, surfaces, volumes, record snapshot, record video, wireframe surfaces, spherical grids with evenly distributed points. For some results see Fig. 9A,B,C and Fig.7A-E. Lights enable as well two types of multithreaded interaction a. a graphical user interface using wxWindows and the 3d interaction that enables the user to translate the volumes and other primitives.

The diffusion module calculates at the moment the SDT (tensorfitsimple), generates FA results. The future version of diffusion will be able to generate probabilistic tracts. The eyes module is an alternative visualisation module that enables very fast tractography representation and interaction. Imagine that the data sets we have contain hundreds of thousands of trajectories. To be able to depict them and interact with them in a user friendly speed is a difficult problem, see Fig. 9D.

The form module loads and writes many different types of files. For example Nifti, Analyze, Dicom, files with diffusion gradient directions (bvecs) and b-values (bvals), DTK tractography files e.g. trk files and also reads Excel files. It has also the possibility to compress and decompress files.

The art module is related with the development and testing of new artificial intelligence or machine learning algorithms and the use of existing ones. At the moment art uses the Modular Toolkit (MDP) e.g. to generate FastICA and Scipy for optimisation & integration methods.

Finally, the external module is used mainly as an alternative of bash scripting calling different external tools.

TRN Modules	Main Features
lights.py	3D/4D visualisation using VTK & GUI using wxWindows
diffusion.py	Calculate Tensors & FA
eyes.py	OpenGL & Fast Tractography visualisation
form.py	File Reading & Writing
art.py	Machine Learning & Artificial Intelligence
external.py	Wrappers for external tools e.g. DTK, mri_convert.

Table 2: Summary of the developed features in TRN.

For example it can generate tractography using DTK, convert files using mri_convert, find files, list directories etc. In the near future we plan to wrap FSL, Camino, Freesurfer commands.

There are many specific very interesting details about the software and the algorithms that we used that cannot be added in this short report. However we are planning write a small wiki for other people to start using them in the MRC-CBU. Dr. Hampshire is already keen on using lights for his own visualisation problems.

6 FA Results

During our journey on understanding the underlying theory behind dMRI methods we had to spend a lot of time trying to figure out the merits and deficits of the classical SDT approaches using FA volumes. In the next paragraph we present some exciting results we had during this enrolment.

6.1 Trichotillomania

Trichotillomania is a disease with the symptom of impulsive hair pulling. It is also a disease that very little imaging data have been published. Chamberlain et al. [18] showed grey matter abnormalities in anterior congulate cortex and pre SMA. In collaboration with Adam Hampshire from MRC-CBU we tried to confirm and extend this result using diffusion imaging. The quality of the data sets was not good enough to generate tractography but they were good enough to calculate and analyse fractional anisotropy (FA) images. We found 3 clusters of lowered FA in the trichotillomania group compared with controls. A white matter cluster under the preSMA and ACC, mostly in the right hemisphere, another white matter cluster under the left hemisphere in the hand area of the pre motor cortex and a large cluster in left hemisphere that spread from underneath the pre motor cortex. These results are planned to be published at the Journal of American Psychiatry. My contributions was mainly on planning the diffusion analysis and visualising the data sets using our new software TRN. In the beginning we tried to use FSL for all the analysis however we had better results when combined FSL, SPM & CAMBA. This was inspired by a previous work of Chamberlain et al. with an OCD study[41].

The data set included 20 patients with trichotillomania and 20 matched controls. Data collected at the MRIS in Addenbrooks on the 1.5 T GE Signa scanner using 25 gradient directions and one volume with b=0. MPRAGE was also collected. More information about the acquisition protocol and parameters can be found here[41].

Eddy correction and calculations of FA maps carried out in FSL/FDT and followed the standard on line directions. Then, for each participant, the b0 was co-registered with the MPRAGE and this transform was applied to the FA maps. The MPRAGE was co-registered and normalised to the MNI template in SPM5 and these parameters were applied to the FA maps. The FA maps were now in the same space as the MNI template in SPM5. A spatial smooth was applied to the FA maps in SPM 5 using an 8mm Gaussian kernel. Group level analysis were carried out in CAMBA using cluster level correction. A white matter mask was obtained (from Sam Chamberlains previous OCD study). This white matter mask was defined by binarising the Statistical Parametric Mapping a priori white matter template to a binary mask, i.e., thresholding each voxel at 50% white matter to define white matter regions for analysis. FA maps were then compared cross group and within the white matter mask using a threshold of $p < 1$ false positive and two tailed cluster analysis.

For the visualisation of the results we used Freesurfer to extract the cortical surface from the MNI template. Then we used our own TRN software for the visualisation. The cortical surface was plotted using surface and contour rendering and the FA clusters were plotted inside the cortical surface using volumetric rendering. See Fig. 9A. For more information about how this visualisation was possible look section Software. We are now

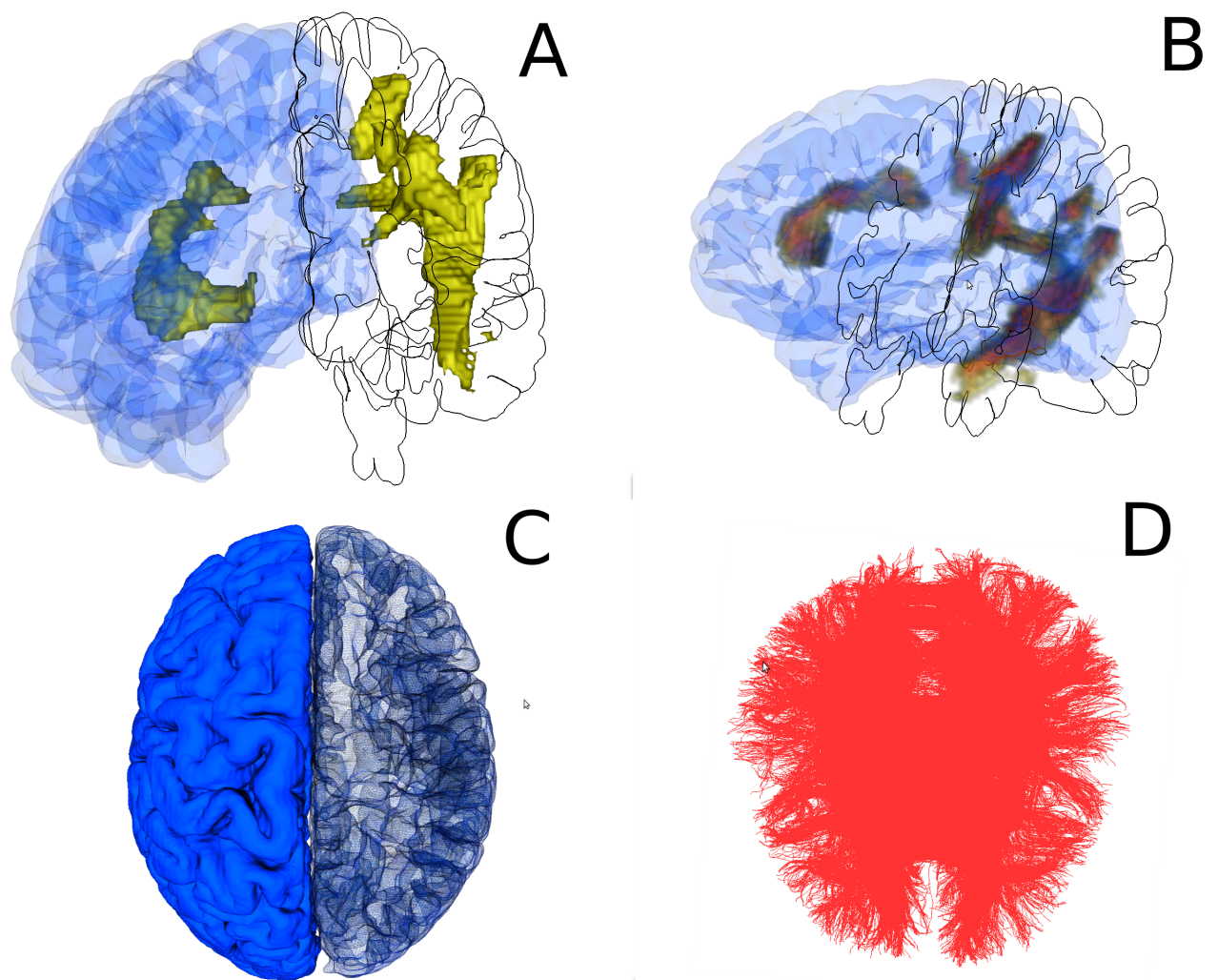


Figure 9: A, B, C are produced by TRN lights & D is generated using TRN eyes. Data set where loaded using TRN form. A,B & C show results found from the Trichotillomania experiment and D depicts fibre tracts without any orientation colour coding.

Acquisition	b-value	directions	repetitions
1A	1000	64	1
2A	3000	64	1
3A	5000	64	1
4A	5000	12	5

Table 3: Summary of the different acquisitions.

under the process with Dr. Adam Hampshire of making this graphical process automated so we can use it in all our following analyses that combine volumetric with surface data. The difficult part usually to achieve this is how to register these two data sets together. However, this is high too technical and complicated for this report.

We are running a larger cohort during Autumn 2009 with higher resolution sequence and we will also be collecting functional fMRI data in this patient group for the first time. We plan to identify functional differences and generate beautiful and hopefully meaningful tracts that will confirm our FA results.

7 Tractography Results

Here we discuss about some inspiring results he had using our new tractography optimised acquisitions.

7.1 HARDI Experiments in CBU

The default Siemens diffusion acquisition protocol that we are using in CBU uses a rectangular voxel size of $1.8 \times 1.8 \times 2.5 \text{ mm}$. We found that this creates problems with many different tractography software e.g. DSI Studio developed by Fang-Cheng Yeh. Tractography algorithms prefer cubic voxel size because that simplifies the modelling, clustering and interpolation of the tracts. This change would simplify as well our free model ideas described in section 8. Furthermore, we were planning to test the accuracy of tractography using acquisitions with different b-values. After some fruitful discussions with Dr. Guy Williams, Dr. Christian Schwarzbauer we decided to run 4 acquisition schemes using 2 subjects and some fruits. All acquisitions were held in our own MRC-CBU's Siemens Trio scanner.

The first acquisition (1A) was using the following parameters: voxel size $2.0 \times 2.0 \times 2.0 \text{ mm}$, 64 directions, slice thickness 2.0 mm , TR=9200 ms, TE=93 ms, FoV read 256 mm and b-value= 1000 s/mm^2 . One more volume was acquired with b-value = 0 s/mm^2 . The total duration of the experiment was 10 minutes and 27 seconds.

The second acquisition (2A) was exactly the same with the previous one but using b-value = 3000 s/mm^2 , TR=10600 ms and TE= 114 ms. The total duration was 12 min and 27 sec.

The third acquisition (3A) was the same with the previous two but using b-value = 5000 s/mm^2 , TR=11500 ms and TE = 127 ms. The total duration was 13 min and 4 sec.

All the first three acquisitions were using 64 directions but the fourth one (4A) was using 12 directions with b-value 5000 s/mm^2 and the following parameters: TR=11500 ms, TE=127 ms, Averages=5. Table 3 summarises their main differences.

Unfortunately, the scanner failed to run 3A and 4A because of overheating problems. We believe that it is very important to gather data with high b-values because in that way we will be able to use algorithms that provide very detailed tractography e.g. QBI [56], EQBI [16] and DSI[57]. We are expecting technical experts from Siemens to solve this problem very soon hopefully during the summer. Furthermore, we scanned some fruits and vegetables with fibre structure e.g. a mango and a pineapple but the signal was too weak to be useful for tractography validation.

However, from 1A and 2A we gathered tracts using software and get the beautiful and inspiring results shown in figures 1,2,10,7.1

8 Future Plan

Second Year

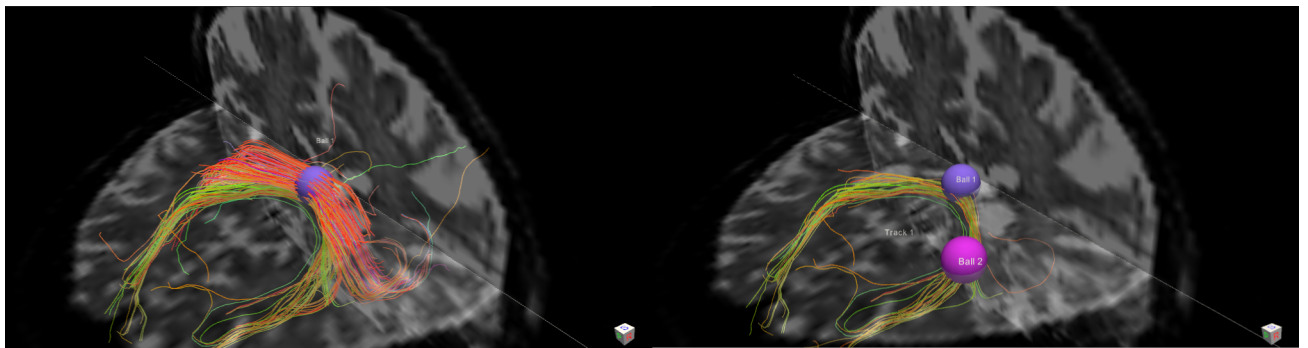


Figure 10: Left: Using one spherical ROI in TrackVis, Right: Using 2 spherical ROIs.

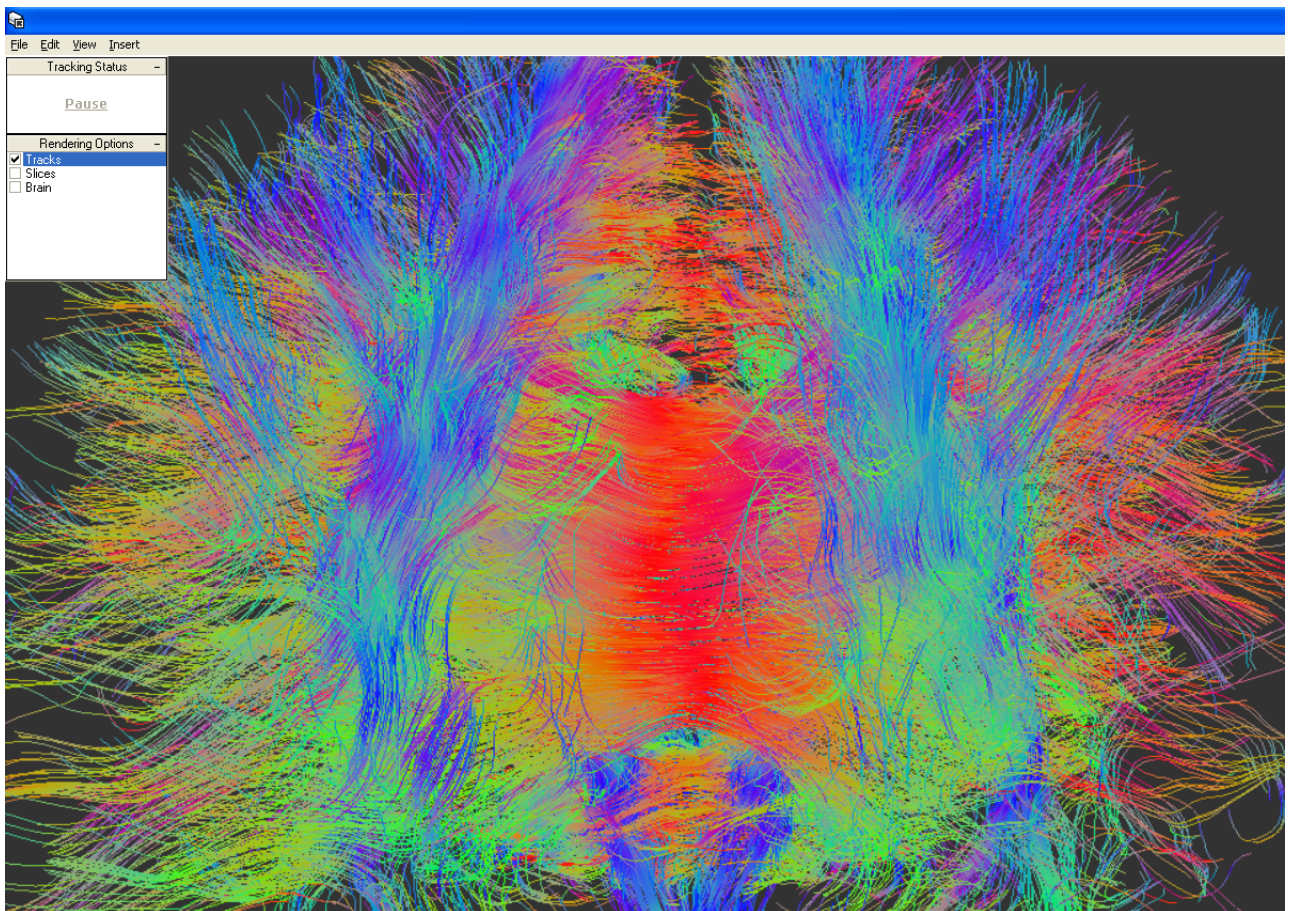


Figure 11: DSI Studio created this result only after changing the acquisition protocol used in CBU. DSI Studios is calculating this deterministic tractography using Runge-Kutta (RK). The colour coding shows the different orientations from the FA image.

1. First priority at the moment is to start implementing our idea for obtaining more information from the actual diffusion signals in each voxel (model free approach avoiding the tensor, multi-tensor and ODF approaches) and use it in a global fashion to denoise our data. We know that in a voxel we can have a nearly infinite number of configurations and patterns. However we believe that with a multidimensional histogram analysis and dimensionality reduction we can find some basic patterns. For a simplified 2D example look Fig. 12. In summary, what we will try to do is a local voxel-based clustering of the signal configurations. In order to reduce the configuration search space we are planning to try first linear dimensionality reduction e.g. PCA and nonlinear dimensionality reduction e.g. Isomap [55] or FastICA[32]. We would like then to cluster the different configurations in discrete patterns as shown in figure 12.

It is important here to note that every configuration is not deterministic but probabilistic enabling for the possibility of errors. Error correction and denoising will be used in a neighbourhood level simultaneously in the hole brain data using discrete optimisation. The discrete optimisation algorithm that we are planning to use is based on the seminal work of Vladimir Kolmogorov[14] in Max-Flow.

Alternative: If the discrete optimisation idea does not show good results we will try to implement and extend the work of Özarslan and Pickalov[49] on fast reconstruction of the diffusion propagator or use compressed sensing[17] that had great success in computerised tomography (CT). The mathematics of CT have many similarities with these of dMRI therefore there is huge potential for algorithmic sharing.

2. After the denoising of our data sets we will try to implement probabilistic tracts which embed prior knowledge in a Bayesian fashion. For example in normal healthy brains there will always be an actual optic radiation underlying our data sets. Could we use this info in a Bayesian way? This idea was inspired by the work of Sherbondy et al[53] explained in section 8. We are also planning to compare the results against many other well known deterministic and probabilistic algorithms e.g. FACT, RK, FSL/FDT and Camino.
3. We are currently writing a review paper in collaboration with Dr. Williams, Dr. Brett, Dr. Nimmo-smith and Dr. Melie-Garcia entitled “Finding connections with diffusion weighted imaging”. We hope that we will be able to finish this paper by the end of September. We are already half way through. The paper is planned to be published at the Journal of Cognitive Neuroscience and the target audience is psychologists not mathematicians or engineers who would like to understand the basics of graph and network theory for dMRI connectivity analysis. Hopefully, this paper will finish before the end of September 2009.
4. We would like to implement a theoretical acquisition model called Exact QBI [16] in the MRC-CBU Siemens scanner which will give us very detailed diffusion data very close to the resolution of DSI. This will be the first time that this model is implemented in a real scanner. However this acquisition depends on multi-shell data with very high b-values up to 10000 and we are waiting from Siemens for an answer if this is eligible in our scanner.

Alternative: There is a high possibility to drop this experiment from taking place at the MRC-CBU and try it at the WBIC where they have a small ball system which enables experiments with enormous gradient switches but unfortunately cannot be used with humans.

Final year

1. In the final year we will concentrate more on finding tracts that are similar across different subjects. Similarity parameters could be the length, curvature, thickness, torsion, distribution of thickness and others. In that way we hope to find solid landmarks that we can use to effectively co-register the subjects using tractography information and not classic FA as in FSL/TBSS.
2. We are also planning to acquire some synthetic or biological phantoms to validate our algorithms. For example Perrin et al. studied a complex phantom made from crossing hemodialysis fibres [48]. We share already some diffusion software phantoms (depicting DNA helices) obtained from UCLA. Unfortunately, global standard validation tools for dMRI are not available widely and this is a problem that we are trying to investigate. Roebroeck et al. [51]used a biological phantom, the optic chiasm in vitro which probably provides the best tissue-based crossing fibre.
3. We would like to combine tractography with surface reconstruction software e.g. Freesurfer and try to use the information from tractography to segment/parcellate the cortex in meaningful areas. Similar work

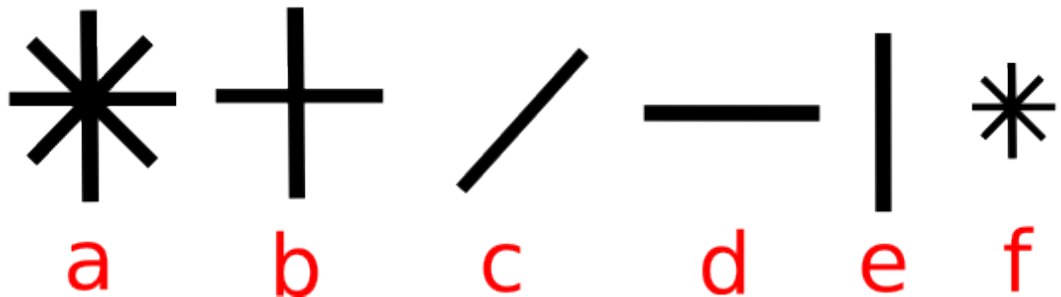


Figure 12: 2D simplified example of some patterns than can be found in a voxel: a) multiple fibre crossing, b) simple fibre crossing, c) diagonal fibre, d) horizontal, e) vertical fibre, f) multiple crossing. The difference in size between f and a means that f is more likely to be an actual crossing because the signal is very low in every direction. Low signal in dMRI means higher directional and less isotropy. Therefore, a is more isotropic than f i.e. f is more likely to be a fiber crossing than a. This is a fact not used at the moment in any other tractography methods.

was already published by Berhens [10]and Perrin [46]. We would like to extend these works using our registration described in 1.

4. Finally write the thesis, publish our results and make our software publicly available.

9 Conclusion

This is the first PhD course in MRC-CBU that is concentrated in diffusion MRI. Most of the time until this day was spent on understanding the theory, using the existing tools and making links and collaborations with other researchers who are more proficient in the field e.g. Dr. Williams on diffusion acquisitions and Dr. Melie-Garcia on connectivity analysis and graph theory. We had also progress developing our own software library in Python named TRN. TRN at the moment is able to calculate simple tensors, read and convert many different medical files, generate very complex graphics e.g. 4D density plots and many more options as described in section 5. We also analysed diffusion data sets using many different tools e.g. TrackVis, DTK, FSL, CAMBA, DSI Studio, Brain Visa, SPM and generated cortical surfaces using Freesurfer. We were happy to see lower FA with patients suffering from trichotillomania (see 6.1) and also generate extensive tractography implementing a new protocol with a cubic voxel size (see fig 1,2) which hopefully will replace the default Siemens protocol used in CBU. Our primary concentration for the future is to investigate and implement a more meaningful tractography using machine learning and discrete optimisation. For this project we collaborate with two researchers from Computer Vision Group, Toshiba Research Laboratory in Cambridge, Dr. Vogiatzis and Dr. Hernández.

Finally, we envision tractography to become in the future the gold standard for registration of different brain modalities as today is the structural MRI and the Tailarach space. We also believe that diffusion tractography has a great potential to become a non-invasive navigation tool for surgical planning. However, current tractography is difficult to validate and visualise and can generate ghosts and artifacts. We are hoping to contribute the maximum towards the solution of these problems in the time left in this course.

10 Acknowledgements

The work established so far would not be possible without the help, encouragement and discussion with the following researchers and students:

Dr. Ian Nimmo-Smith (supervisor MRC-CBU), Dr. Christian Schwarzbauer (2nd-supervisor MRC-CBU), Dr. Guy Williams (Wolfson Brain Imaging Centre - WBIC), Dr. Matthew Brett (Berkeley University), Dr. Lester Melie-García (Cuban Neuroscience Centre), Dr. George Vogiatzis (Toshiba Research), Dr. Carlos Hernández (Toshiba Research), Dr. Adam Hampshire (MRC-CBU), Dr. Mirjana Boszic (MRC-CBU), John Griffiths

(Department of Experimental Psychology), Daniel Wakeman (MRC-CBU) and Hsiao-Lan Sharon Wang (Centre for Neuroscience in Education).

We would like also to thank our sponsors EPSRC, BGS, Vergottis Trust & MRC for all their support providing our resources.

11 Appendix

11.1 Problems for fiber tracking

Of course the fibre tracking algorithms are primarily being affected by the presence of noise. Typically, some of the noise is electronic noise that is added by the scanner and can be well approximated with a Rician distribution[31, 6]. Another noise factor is generated from partial volume effects where inside a voxel we have more than one type of different tissues with different diffusion behaviour. This phenomenon is strengthened a lot as we go closer and closer to the gray matter where the actual fibres are physiologically thinner and the diffusion signal is more isotropic. In the partial volume domain many different fibre configurations take place. The fibres can possibly circulate, cross or kiss, merge or branch, bulge or neck, terminate or kink (discontinuous). Other noise elements get into the final data that are useful for tractography because of misregistration of DWIs caused by eddy currents, ghosting due to motion artifacts and signal loss due to susceptibility variations. Finally, the amount of smoothing or clustering applied to reduce the noise might generate tracks that do not exist anatomically i.e. false connections. However, all the above noise factors can become generators of ghost tracks and it is a very difficult problem today to try to reduce the number of these tracks and validate their results with anatomical maps.

11.2 Motion and Eddy Correction

We describe here a common procedure for registering the different DWIs of the same subject in order to reduce the noise from the subject's motion and eddy currents [34],[28]. For each data set, we construct a reference/template volume by calculating the mean intensity in each voxel from all the non-diffusion weighted images. Next we compute the mutual information between the DWI and the reference image and minimise their difference using a classic optimisation method e.g., the downhill simplex method. Only affine movements are allowed during the registration process. That is because the distortions from the eddy currents can be approximated with stretches and shears in the DWIs.

These distortions are different for every gradient direction. Affine registration corrects for shearing and stretching but corrects as well for head motion because the space of rigid transformations is a subset of the space of affine transformations. Eddy_correct is a tool in FSL/FDT that works in a similar way with what we described above. For more sophisticated approaches see [60] and [1].

A common raised question is how many non-diffusion images do we need for maximal motion correction results. Jones et al. [34] showed that in order to obtain optimal tensor imaging we need approximately 1 non-diffusion volume for every 7.5 diffusion weighted volumes.

Other noise correction strategies include rician noise removal using wavelets [58] and denoising in cardiac DWI using sparse representation[4].

11.3 Comparing across subjects

In structural MRI when we want to compare across subjects we have to compare only between 3D volumes. In diffusion imaging things are much more complicated as we have many 3D volumes for each subject. For example in QBI we might have 515 or more directional volumes. Comparing every single directional volume from two or more subjects is highly impractical as it is very time consuming to process our data sets. Therefore, research groups try to find new ways to reduce the dimensionality while keeping most of the information.

Three main approaches have been used for quantitative inter-subject analysis in diffusion imaging, region of interest ROI-based methods, voxel-based methods, and tract-based methods. The ROI-based methods are by far the most popular in clinical practise. Usually FA is calculated in manually defined ROIs and averaged over groups of healthy and diseased populations e.g. histogram analysis over a ROI. With these methods it is easy

to examine specific hypotheses associated with specific brain disorders. Apart from FA, the mean diffusivity (MD) volumes or primary eigenvalue volumes could be used in a similar fashion.

The disadvantages of ROI-based methods are that they are not time efficient because they require user interaction and their accuracy is confined by the reliability of defining the ROIs. Kanaan et al. [35] showed that the ROI size, shape, number, and location not only affect the measured quantities, but also influence the significance of the group analysis. In voxel-based methods the data sets are compared voxel-by-voxel. These methods are simple but precise alignment is very critical. Registering scalar fields like FA does not employ all of the information in the data and will not provide the most accurate analysis. The advantages of voxel-based methods are that they are user-independent and they are more holistic because they include the whole-brain. Their disadvantages are that smoothing for statistical validity reduces resolution, and significant group differences do not necessarily lie within an anatomical tract. Another important point is that it is relative common to use a DWI-based atlas e.g. Mori Atlas[43]. However, reference to an anatomical atlas is hindered by the low resolution of the obtained difference map by the limited resolution of the atlas itself [35].

Tract-oriented methods offer advantages over ROI-based since they reveal local variations of the fibre integrity which are lost when the quantitative parameters are averaged over the entire fibre tract in ROI-based methods. Clustering techniques are used to group trajectories (tracts) to single fibre bundles. The principal benefit is that observed differences are due to differences in the properties of specific tracts rather than differences in the overall anatomy/shape of the individual brains [38].

Regardless of the nature of tractography methods, whether deterministic or probabilistic, the output trajectories often have discontinuities due to the presence of noise and image imperfections. Even with an ideal tractography algorithm and incredibly efficient pre-processing of the data to remove noise artifacts, lesions and other brain abnormalities may cause discontinuities in the trajectories. Defining similarity between trajectories is not trivial. The similarity between three-dimensional curves (trajectories or tracts) is not uniquely defined and depends on the application. The space of the fibre tracts can variate very much. In deterministic tractography it is relatively common to represent them as a list of paths where every path is a list of points on the diffusion space. Because of the anatomical differences comparing fibre tracts between different subjects is an open problem. A tract that pass through the x,y,z point in subject A doesn't mean it will pass through the same point in subject B. Actually, probably the path will not even start or end to the same points if the subjects have small or profound anatomical differences. Therefore in order to compare tracts we need to use more elaborate properties of the tracks like higher order derivatives, curvature, kurtosity etc. In addition, the general assumption that a fibre tract has one pixel thickness should also be under consideration especially in virtual dissection applications. A good strategy is to require the similarity measure to use both spatial and shape information from the whole trajectory. The point correspondence could be facilitated by the use of landmarks that contain most of the information for the shape and location of trajectory. Such landmarks can be specified using local extrema[23] or minimum description length[21].

An unsupervised algorithm is not easy to produce the clusters of interest for a given application because of over or under-fitting i.e., more or less clusters are generated from the algorithm across subjects and therefore cluster to cluster correspondence is difficult to achieve. Mahnaz Maddah in her thesis used a supervised clustering algorithm with SDT data that benefits from anatomical information. By such a tract-based analysis, she was able to identify a significant drop in FA in the vicinity of the lesion (see [38] p.31), without knowing where the lesion is located a priori. The point correspondence between the trajectories is built using a distance map and a Voronoi diagram on the same space. The anatomical prior is given by an anatomical atlas or by a Dirichlet distribution that controls the impact of the atlas. Another popular method was proposed by Odonell et. al [44] by the name of tract-based morphometry but we will not describe it here.

We stressed in previous sections that FA is very restricted as it doesn't give any directional local information and any crossing or merging is missed. However, some of the major bundles are visible even in FA volumes. Therefore, usually for simplicity most of the current methods use FA to compare across subjects. The idea is to register all FA images together usually on a template that is the mean FA image. Some problems of missing fibres are described here in [24] and for comparison between connections that were visualised using injected neural tract tracer and DWI tractography in the macaque brain [20].

11.4 TBSS

In collaboration with Dr. Boszic we tried to use FSL/TBSS to cor-register many subjects together, define the mask in the mean FA image and then using TBSS de-project go back to the native diffusion space and do

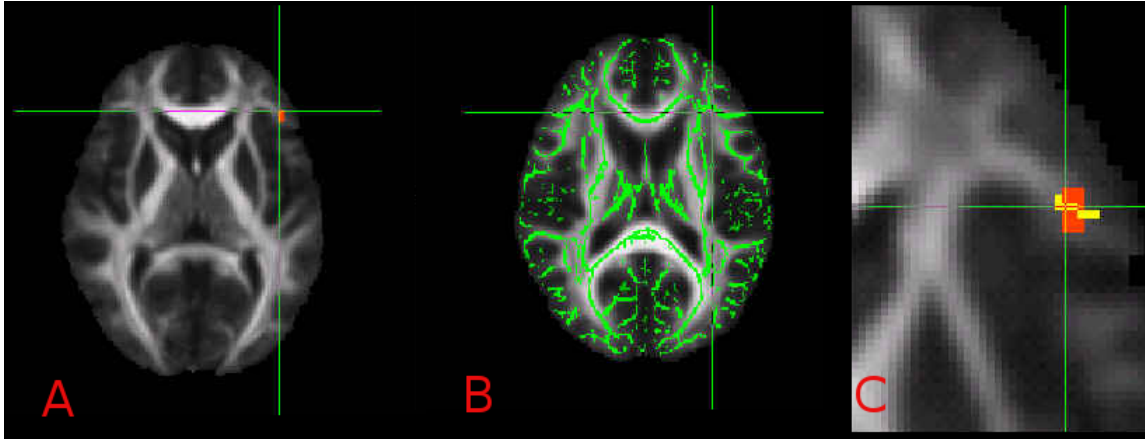


Figure 13: A: FA slice and seed, B: TBSS skeleton, C: After de-projection the masks were broken or very much de-morphed.

tractography there. We tried this idea because it is very time consuming to define seeds in every single subject it could take many weeks and it can be very biased. So, this automation idea could have reduced our analysis time dramatically. Unfortunately, the nonlinear nature of TBSS and the high dependence on the skeleton was not able to de-project the masks efficiently i.e. many masks were broken. We hope that in future versions of TBSS this will be resolved.

11.5 Visualising local estimates of diffusion direction

In order to get useful inter-voxel information from DWI data it is necessary to create some sort of model for the local directional dependence of the diffusion weighted MR signal. The models investigated to date involve a range of physical assumptions about the complexity of the structure of the tissue. There are several ways of displaying the estimated diffusion direction distributions.

11.5.1 Tensor models

Single diffusion tensor

The best known, the single diffusion tensor (SDT) model was also the first to be published[7]. SDT is also sometimes called the *simple* diffusion tensor model. The term single diffusion tensor is more useful, by contrast with multi-tensor models (see below). First principal direction identified with direction of fibre. Problems identified with non-positivity of standard regression method of fitting. More seriously it breaks down when there are fibres crossing. The SDT model is very simple, and assumes homogeneity and linearity of the diffusion within each image voxel. The model requires six, or more gradient directions, sufficient to compute the diffusion tensor. From the diffusion tensor, diffusion anisotropy measures such as the FA, can be computed. Moreover, the principal direction of the diffusion tensor can be used to infer the white-matter connectivity of the brain (See section 8).

Higher order tensors

Higher order non-negative tensor models [5] are algebraic extensions which model the logarithm of the signal as a non-negative symmetric polynomial of degree 4 (quartic) in the components of the gradient vector, by analogy with SDT which is equivalent to fitting a symmetric polynomial of degree 2. No attempt at a physical analogy to justify. The parameters do not yet have well formulated interpretations in relation to the geometry of the corresponding fitted function. However a 'generalised trace' measure has been advanced as an analogy of the classical apparent diffusivity coefficient (ADC).

Multi-tensor models

There are a number of multi-tensor models to consider. Sometimes called multi-compartment by analogy with statistical thermodynamics. Usually an isotropic component and one or more anisotropic tensor component. Sometimes the latter are explicitly reduced to degenerate uni-dimensional compartments[12],[36].

11.5.2 Spherical Harmonic Models

SDT as originally formulated was expected to be based on a small or medium number of gradient volumes. The development of new faster MR sequences has meant that data can be collected in a realistic timescale from a very large number of gradients. These techniques (HARDI, Q-ball etc.) thus can sample the signal as a function of the \mathbf{q} at a large number of locations in \mathbf{q} -space. This in turn allows for smoothing and interpolation with a function which is a finite linear combination of basis functions (spherical harmonics) which are the 'natural' analogues of Fourier smoothing for a function of a single variable.

11.5.3 Model free

The term model free is used here to stress that there is no assumption for the probability displacement distribution in the voxel. So, it means either that we are using either the full propagator that needs too many directions e.g. as used in DSI or use the default signal as it is. For example, if we were applying 60 diffusion directions the model free approach would imply that every voxel would correspond a multidimensional vector with 60 values. The model free approach is of great interest to us as we believe that will generate better tractography than the model based methods used until today. See section 8 for more.

References

- [1] J.L.R. Andersson and S. Skare. A model-based method for retrospective correction of geometric distortions in diffusion-weighted EPI. *Neuroimage*, 16(1):177–199, 2002.
- [2] A. Anwander, M. Tittgemeyer, D Y von Cramon, A D Friederici, and T R Knosche. Connectivity-Based Parcellation of Broca’s Area. *Cerebral Cortex*, 17(4):816, 2007.
- [3] E. J. Auerbach and K. Ugurbil. Improvement in diffusion mri at 3t and beyond with the twice-refocused adiabatic spin echo (trase) sequence. 2004.
- [4] LJ Bao, YM Zhu, WY Liu, P. Croisille, ZB Pu, M. Robini, and IE Magnin. Denoising human cardiac diffusion tensor magnetic resonance images using sparse representation combined with segmentation. *Physics in Medicine and Biology*, 54(6):1435–1456, 2009.
- [5] A. Barmpoutis, B. C. Vemuri, T. M. Shepherd, and J. R. Forder. Tensor splines for interpolation and approximation of {DT-MRI} with applications to segmentation of isolated rat hippocampi. *IEEE Transactions on Medical Imaging*, 26(11):1537–1546, 2007.
- [6] P. J. Basser, S. Pajevic, C. Pierpaoli, J. Duda, and A. Aldroubi. In vivo fiber tractography using DT-MRI data. *Magn Reson Med*, 44(4):625–32, 2000.
- [7] Peter J. Basser, James Mattiello, and Denis LeBihan. MR diffusion tensor spectroscopy and imaging. *Biophysical Journal*, 66:259–267, 1994.
- [8] C. Beaulieu. The basis of anisotropic water diffusion in the nervous system - a technical review. *NMR Biomed*, 15(7-8):435–55, 2002.
- [9] T E Behrens and H. Johansen-Berg. Relating connectional architecture to grey matter function using diffusion imaging. *Philos Trans R Soc Lond B Biol Sci*, 360(1457):903–11, 2005.
- [10] T E J Behrens, H Johansen-Berg, M W Woolrich, C A M Wheeler-Kingshott, P A Boulby, G J Barker, E L Sillery, K Sheehan, O Ciccarelli, A J Thompson, J M Brady, and P M Matthews. Non-invasive mapping of connections between human thalamus and cortex using diffusion imaging. *Nature Neuroscience*, 6(7):750–757, 2003.

- [11] T. E. J. Behrens, M. W. Woolrich, M. Jenkinson, H. Johansen-Berg, R. G. Nunes, S. Clare, P. M. Matthews, J. M. Brady, and S. M. Smith. Characterization and propagation of uncertainty in diffusion-weighted {MR} imaging. *Magnetic Resonance in Medicine*, 50:1077–1088, 2003.
- [12] T.E.J. Behrens, H. Johansen-Berg, S. Jbabdi, M.F.S. Rushworth, and M.W. Woolrich. Probabilistic diffusion tractography with multiple fibre orientations: What can we gain? *NeuroImage*, 34(1):144–155, 2007.
- [13] M. Björnemo, A. Brun, R. Kikinis, and C.-F. Westin. Regularized stochastic white matter tractography using diffusion tensor MRI. In *Fifth International Conference on Medical Image Computing and Computer-Assisted Intervention (MICCAI'02)*, pages 435–442, Tokyo, Japan, 2002.
- [14] Y. Boykov and V. Kolmogorov. An experimental comparison of min-cut/max-flow algorithms for energy minimization in vision. *IEEE Transactions on Pattern Analysis and Machine Intelligence*, 26(9):1124–1137, 2004.
- [15] Paul T. Callaghan. *Principles of Nuclear Magnetic Resonance Microscopy*. Oxford University Press, 1991.
- [16] E.J. Canales-Rodríguez, L. Melie-García, Y. Iturria-Medina, and C.N. Center. Mathematical description of q-space in spherical coordinates: Exact q-ball imaging. *Magnetic resonance in medicine: official journal of the Society of Magnetic Resonance in Medicine/Society of Magnetic Resonance in Medicine*, 2009.
- [17] E.J. Candès and M.B. Wakin. An introduction to compressive sampling. *IEEE Signal Processing Magazine*, 25(2):21–30, 2008.
- [18] S.R. Chamberlain, L.A. Menzies, N.A. Fineberg, N. del Campo, J. Suckling, K. Craig, U. Müller, T.W. Robbins, E.T. Bullmore, and B.J. Sahakian. Grey matter abnormalities in trichotillomania: morphometric magnetic resonance imaging study. *The British Journal of Psychiatry*, 193(3):216–221, 2008.
- [19] T. E. Conturo, N. F. Lori, T. S. Cull, E. Akbudak, A. Z. Snyder, J. S. Shimony, R. C. McKinstry, H. Burton, and M. E. Raichle. Tracking neuronal fiber pathways in the living human brain. *Proc Natl Acad Sci U S A*, 96(18):10422–7, 1999.
- [20] J. Dauguet, S. Peled, V. Berezovskii, T. Delzescaux, S. K. Warfield, R. Born, and C. F. Westin. Comparison of fiber tracts derived from in-vivo DTI tractography with 3D histological neural tract tracer reconstruction on a macaque brain. *Neuroimage*, 37(2):530–8, 2007.
- [21] R. H. Davies, C. J. Twining, T. F. Cootes, J. C. Waterton, and C. J. Taylor. A minimum description length approach to statistical shape modeling. *IEEE Trans Med Imaging*, 21(5):525–37, 2002.
- [22] MD Denis Le Bihan, C. Poupon, A. Amadon, and F. Lethimonnier. Artifacts and pitfalls in diffusion MRI. *Journal of Magnetic Resonance Imaging*, 24:478–488, 2006.
- [23] R. Deriche and O. Faugeras. 2-D curve matching using high curvature points: application to stereo vision. In *Pattern Recognition, 1990. Proceedings., 10th International Conference on*, volume 1, 1990.
- [24] R. F. Dougherty, M. Ben-Shachar, R. Bammer, A. A. Brewer, and B. A. Wandell. Functional organization of human occipital-callosal fiber tracts. *Proc Natl Acad Sci U S A*, 102(20):7350–5, 2005.
- [25] A. Einstein. *Investigations on the Theory of the Brownian Movement*. Dover Publications, 1956.
- [26] O. Friman and C. F. Westin. Uncertainty in white matter fiber tractography. *Med Image Comput Comput Assist Interv Int Conf Med Image Comput Comput Assist Interv*, 8(Pt 1):107–14, 2005.
- [27] P. Hagmann, J. P. Thiran, L. Jonasson, P. Vanderghenst, S. Clarke, P. Maeder, and R. Meuli. DTI mapping of human brain connectivity: statistical fibre tracking and virtual dissection. *Neuroimage*, 19(3):545–54, 2003.
- [28] J. C. Haselgrove and J. R. Moore. Correction for distortion of echo-planar images used to calculate the apparent diffusion coefficient. *Magn Reson Med*, 36(6):960–4, 1996.
- [29] O. Heid. Eddy current-nulled diffusion weighting. In: *Proceedings of the 8th Annual Meeting of ISMRM, Denver*, page 799, 2000.

- [30] Heidi Johansen-Berg. *Diffusion MRI*. Academic Press, 2009.
- [31] T. Hosey, G. Williams, and R. Ansorge. Inference of multiple fiber orientations in high angular resolution diffusion imaging. *Magnetic Resonance in Medicine*, 54(6):1480–1489, 2005.
- [32] A. Hyvärinen and E. Oja. Independent component analysis: algorithms and applications. *Neural networks*, 13(4-5):411–430, 2000.
- [33] S. Jbabdi, MW Woolrich, JLR Andersson, and TEJ Behrens. A Bayesian framework for global tractography. *Neuroimage*, 37(1):116–129, 2007.
- [34] DK Jones, MA Horsfield, and A. Simmons. Optimal strategies for measuring diffusion in anisotropic systems by magnetic resonance imaging. *optimization*, 525, 1999.
- [35] R. A. Kanaan, S. S. Shergill, G. J. Barker, M. Catani, V. W. Ng, R. Howard, P. K. McGuire, and D. K. Jones. Tract-specific anisotropy measurements in diffusion tensor imaging. *Psychiatry Res*, 146(1):73–82, 2006.
- [36] B. W. Kreher, I. Mader, and V. G. Kiselev. Gibbs tracking: A novel approach for the reconstruction of neuronal pathways. *Proc. Intl. Soc. Mag. Reson. Med.*, 16:425, 2008.
- [37] M. Lazar, D. M. Weinstein, J. S. Tsuruda, K. M. Hasan, K. Arfanakis, M. E. Meyerand, B. Badie, H. A. Rowley, V. Haughton, A. Field, and A. L. Alexander. White matter tractography using diffusion tensor deflection. *Hum Brain Mapp*, 18(4):306–21, 2003.
- [38] M. Maddah. *Quantitative Analysis of Cerebral White Matter Anatomy from Diffusion MRI*. PhD thesis, Massachusetts Institute of Technology, 2008.
- [39] G. Margolis and JP Pickett. New applications of the Luxol fast blue myelin stain. *Laboratory investigation; a journal of technical methods and pathology*, 5(6):459.
- [40] D.W. McRobbie, E.A. Moore, and M.J. Graves. *MRI from Picture to Proton*. Cambridge University Press, 2006.
- [41] L. Menzies, G.B. Williams, S.R. Chamberlain, C. Ooi, N. Fineberg, J. Suckling, B.J. Sahakian, T.W. Robbins, and E.T. Bullmore. White matter abnormalities in patients with obsessive-compulsive disorder and their first-degree relatives. *American Journal of Psychiatry*, 165(10):1308, 2008.
- [42] S. Mori, B. J. Crain, V. P. Chacko, and P. C. van Zijl. Three-dimensional tracking of axonal projections in the brain by magnetic resonance imaging. *Ann Neurol*, 45(2):265–9, 1999.
- [43] S. Mori, S. Wakana, LM Nagae-Poetscher, and PCM Van Zijl. MRI atlas of human white matter. *American Journal of Neuroradiology*.
- [44] L. J. O'Donnell, C. F. Westin, and A. J. Golby. Tract-based morphometry for white matter group analysis. *Neuroimage*, 45(3):832–44, 2009.
- [45] G. J. Parker, H. A. Haroon, and C. A. Wheeler-Kingshott. A framework for a streamline-based probabilistic index of connectivity (PICo) using a structural interpretation of MRI diffusion measurements. *J Magn Reson Imaging*, 18(2):242–54, 2003.
- [46] M. Perrin, Y. Cointepas, A. Cachia, C. Poupon, B. Thirion, D. Riviere, P. Cathier, V. El Kouby, A. Constantinesco, D. Le Bihan, and J. F. Mangin. Connectivity-Based Parcellation of the Cortical Mantle Using q-Ball Diffusion Imaging. *Int J Biomed Imaging*, 2008:368406, 2008.
- [47] M. Perrin, C. Poupon, Y. Cointepas, B. Rieul, N. Golestan, C. Pallier, D. Riviere, A. Constantinesco, D. Le Bihan, and J. F. Mangin. Fiber tracking in q-ball fields using regularized particle trajectories. *Inf Process Med Imaging*, 19:52–63, 2005.
- [48] Muriel Perrin, Cyril Poupon, Bernard Rieul, Patrick Leroux, André Constantinesco, Jean-François Mangin, and Denis LeBihan. Validation of q-ball imaging with a diffusion fibre-crossing phantom on a clinical scanner. *Philosophical Transactions of the Royal Society B: Biological Sciences*, 360(1457):881–91, 2005.

- [49] V. Pickalov and P.J. Basser. 3d tomographic reconstruction of the average propagator from mri data. In *3rd IEEE International Symposium on Biomedical Imaging: Nano to Macro, 2006*, pages 710–713, 2006.
- [50] T.G. Reese, O. Heid, R.M. Weisskoff, and V.J. Wedeen. Reduction of eddy-current-induced distortion in diffusion mri using a twice-refocused spin echo. *Magnetic Resonance in Medicine*, 49(1):177–182, 2003.
- [51] A. Roebroeck, R. Galuske, E. Formisano, O. Chiry, H. Bratzke, I. Ronen, D. Kim, and R. Goebel. High-resolution diffusion tensor imaging and tractography of the human optic chiasm at 9.4 T. *Neuroimage*, 39(1):157–168, 2008.
- [52] AJ Sherbondy, DL Akers, RF Dougherty, M. Ben-Shachar, S. Napel, and BA Wandell. MetroTrac: A metropolis algorithm for probabilistic tractography. *Human Brain Mapping, Florence*, 2006.
- [53] Anthony J. Sherbondy, Robert F. Dougherty, Michal Ben-Shachar, Sandy Napel, and Brian A. Wandell. ConTrack: Finding the most likely pathways between brain regions using diffusion tractography. *J. Vis.*, 8(9):1–16, 7 2008.
- [54] E. O. Stejskal and J. E. Tanner. Spin diffusion measurements: Spin echoes in the presence of a time-dependent field gradient. *The Journal of Chemical Physics*, 42(1):288–292, 1965.
- [55] J.B. Tenenbaum, V. Silva, and J.C. Langford. A global geometric framework for nonlinear dimensionality reduction, 2000.
- [56] D.S. Tuch. *Diffusion {MRI} of complex tissue structure*. PhD thesis, Massachusetts Institute of Technology, Division of Health Sciences and Technology, 2002.
- [57] V. J. Wedeen, R. P. Wang, J. D. Schmahmann, T. Benner, W. Y. Tseng, G. Dai, D. N. Pandya, P. Hagmann, H. D'Arceuil, and A. J. de Crespigny. Diffusion spectrum magnetic resonance imaging (DSI) tractography of crossing fibers. *Neuroimage*, 41(4):1267–77, 2008.
- [58] R. Wirestam, A. Bibic, J. Latt, S. Brockstedt, and F. Stahlberg. Denoising of complex MRI data by wavelet-domain filtering: Application to high-b-value diffusion-weighted imaging. *Magnetic Resonance in Medicine*, 56(5), 2006.
- [59] G. Zhai, W. Lin, K. P. Wilber, G. Gerig, and J. H. Gilmore. Comparisons of regional white matter diffusion in healthy neonates and adults performed with a 3.0-T head-only MR imaging unit. *Radiology*, 229(3):673–81, 2003.
- [60] J. Zhuang, J. Hrabe, A. Kangarlu, D. Xu, R. Bansal, C. A. Branch, and B. S. Peterson. Correction of eddy-current distortions in diffusion tensor images using the known directions and strengths of diffusion gradients. *J Magn Reson Imaging*, 24(5):1188–93, 2006.